A theoretical and simulation study of the self-assembly of a binary blend of diblock copolymers

Poornima Padmanabhan, Francisco J. Martinez-Veracoechea, Juan C. Araque, and Fernando A. Escobedo

Citation: J. Chem. Phys. **136**, 234905 (2012); doi: 10.1063/1.4729159
View online: http://dx.doi.org/10.1063/1.4729159
View Table of Contents: http://jcp.aip.org/resource/1/JCPSA6/v136/i23
Published by the AIP Publishing LLC.

A theoretical and simulation study of the self-assembly of a binary blend of diblock copolymers

Poornima Padmanabhan,[1] Francisco J. Martinez-Veracoechea,[2] Juan C. Araque,[1] and Fernando A. Escobedo[1,a)]
[1]*Chemical and Biomolecular Engineering, Cornell University, Ithaca, New York 14853, USA*
[2]*Department of Chemistry, University of Cambridge, Lensfield Road, Cambridge, CB2 1EW, United Kingdom*

(Received 22 December 2011; accepted 25 May 2012; published online 19 June 2012)

Pure diblock copolymer melts exhibit a narrow range of conditions at which bicontinuous and cocontinuous phases are stable; such conditions and the morphology of such phases can be tuned by the use of additives. In this work, we have studied a bidisperse system of diblock copolymers using theory and simulation. In particular, we elucidated how a short, lamellar-forming diblock copolymer modifies the phase behavior of a longer, cylinder-forming diblock copolymer. In a narrow range of intermediate compositions, self-consistent field theory predicts the formation of a gyroid phase although particle-based simulations show that three phases compete: the gyroid phase, a disordered cocontinuous phase, and the cylinder phase, all having free energies within error bars of each other. Former experimental studies of a similar system have yielded an unidentified, partially irregular bicontinuous phase, and our simulations suggest that at such conditions the formation of a partially transformed network phase is indeed plausible. Close examination of the spatial distribution of chains reveals that packing frustration (manifested by chain stretching and low density spots) occurs in the majority-block domains of the three competing phases simulated. In all cases, a double interface around the minority-block domains is also detected with the outer one formed by the short chains, and the inner one formed by the longer chains. © *2012 American Institute of Physics*. [http://dx.doi.org/10.1063/1.4729159]

I. INTRODUCTION

Diblock copolymers "DBCs" are linear polymers made up of two types of homopolymers or blocks joined end-to-end. Due to the chemical incompatibility between the monomers, they tend to segregate but cannot do so at the macroscale because of their intramolecular linkage. Exploiting such a tendency for microphase segregation, block copolymers have been used for nanotemplating materials useful in lithography and the synthesis of nanoporous structures for multiple applications including catalysts and solar cell active layers. Of particular interest are bi- and cocontinuous phases that have three-dimensional symmetry, with continuous domains of the different block types. These phases have superior electrical, mechanical, and optical properties[1–3] which are essentially isotropic; i.e., they do not depend on a particular alignment of the morphology with respect to external interfaces. This is because, bicontinuous and cocontinuous phases have either two interweaving (bicontinuous) networks or a single (cocontinuous) network, of the minority block embedded in a matrix of the majority block.

Unfavorable enthalpic interactions in DBCs drive the formation of interfaces during microphase segregation, restricting the junction points of the two different blocks to lie near the interface. On the one hand, formation of the interface localizes sections of the DBC chains reducing the configurations they can explore and hence the entropy. On the other hand, the interface tends to curve towards the minority domain allowing the blocks to balance the amount of stretching required to fill the space. The interplay between these interactions determines the stable microphase.[4]

The confluence of results from experiments and self consistent field theory (SCFT) has led to a detailed understanding of the phase diagram of a pure melt of DBCs.[5] Under some approximations, such a phase diagram is completely described by two parameters: The volume fraction of one of the components f, and the product of Flory-Huggins' interaction parameter and the degree of polymerization χN. The phases found to be stable (over particular f-χN regions) are the micellar (body-centered-cubic and close-packed), cylindrical (hexagonally packed), gyroid, and lamellar phases. Recent SCFT calculations have resolved another fifth stable phase[6] of cocontinuous morphology, which has subsequently been observed in experiments.[7]

The incorporation of an additional species to a DBC melt adds more dimensions to the phase diagram, although it also opens up the possibility of macrophase separation. Nevertheless, the new dimensions potentially allow a larger window of stability of the desired phases and perhaps conditions more accessible via experiments. In particular, adding a second DBC made of the same chemical species forces both species to share the interface; such an additive is often referred to as the "cosurfactant." Shi and Noolandi[8] first studied the effect of adding a very small amount of surfactant and analytically studied the change in interfacial tension and its contribution to the free energy. Early work focused on polymers of the same total degree of polymerization but different block lengths

a)Electronic mail: fe13@cornell.edu.

(allowing a common χN value for the system). For dilute blends, a one-component approximation was shown to be valid using theory.[9] Later studies on blends over a wide range of compositions have mapped out macrophase separation and two-phase coexistence, but they were restricted to the cylinder, lamellar, micellar, and disordered phases only, and did not consider the gyroid phase or other bicontinuous and cocontinuous phases.[10,11]

Experiments have shown that it is possible to obtain bicontinuous and cocontinuous phases by blending suitable DBCs—typically an asymmetric copolymer and a symmetric copolymer.[12–14] It was also shown that blending two symmetric DBCs does not always lead to a lamellar phase, but also to a spongy phase. Hashimoto and co-workers[13,14] studied a binary blend of asymmetric and symmetric DBCs in detail, and found an unidentified bicontinuous phase in between cylinder and lamellae. Spontak *et al.*[12] studied a bidisperse blend of DBCs and found a similar behavior, a cylinder to gyroid to lamellar transition upon increase of overall volume fraction of the minority domain. The preparation method was also found to be critical in determining the observable morphology of the binary blends.[15] Previous simulations[16] have shown that for a bidisperse system of carefully chosen composition, the region of stability of the gyroid phase is enhanced due to the preferential arrangement of the longer diblock at the nodes of the gyroid network.

The present work explores via SCFT and particle-based simulation the phase behavior of a binary blend of DBCs consisting, as in former experimental systems, of a longer asymmetric DBC and a shorter, symmetric DBC. A specific goal is to complement previous experimental observations to clarify, in particular, the stability of the gyroid phase vs. other bicontinuous or cocontinuous phases, an issue that was left unresolved in the study of Court and Hashimoto.[13] We find that while SCFT does predict the existence of a narrow composition range where the gyroid phase is stable, particle-based simulations are unable to resolve among the gyroid phase, cylindrical phase, and a disordered cocontinuous phase. The latter simulations also reveal that such a result is partially due to the existence of packing frustration in the majority-block domains of the gyroid phase.

II. SIMULATION METHODS

A. Self-consistent field theory

In SCFT, polymer chains are modeled as flexible Gaussian chains. The main idea is to replace the calculation of the partition function of the entire system by the calculation of the partition function of a single chain in an external field. Here, we describe the theory for a bidisperse block copolymer blend. For each component c in the blend, the degree of polymerization is N_c and the volume fraction of monomer of type A is f_c, with φ_c the overall volume fraction of the component. χ is the Flory-Huggins interaction parameter between unlike monomers A and B, and N is the chain length of one of the components chosen as the reference. The set of equations for the external fields for the canonical ensemble are[4–6]

$$\omega_A(r) = \chi N \phi_B(r) + \xi(r), \tag{1}$$

$$\omega_B(r) = \chi N \phi_A(r) + \xi(r), \tag{2}$$

$$\phi_A(r) + \phi_B(r) = 1, \tag{3}$$

where ϕ_i are local density fields that satisfy the incompressibility condition Eq. (3), $\xi(\boldsymbol{r})$ is the Lagrange multiplier introduced to enact the incompressibility constraint, and $\omega_i(\boldsymbol{r})$ is the external field that acts on a subunit of monomer type i. The chain propagators "q" obey a diffusion-type of equation,

$$\frac{\partial q_c(r,s)}{\partial s} = \frac{b_i^2 N_c}{6}\nabla^2 q_c(r,s) - \omega_i(r,s) q_c(r,s) \tag{4}$$

for each component c in the blend, b is the Kuhn length, s is a contour variable between 0 and 1 specifying position along the polymer chain, and i denotes the identity of the block along the contour length of the chain. Hence,

$$i = \begin{cases} A, & s < f_c \\ B, & s > f_c \end{cases}. \tag{5}$$

The density fields are calculated as

$$\frac{\phi_A(r)}{N} = \sum\nolimits_c \frac{\varphi_c}{N_c Q_c}\int_0^{f_c} ds q_c(r,s) q_c^+(r,s), \tag{6}$$

$$\frac{\phi_B(r)}{N} = \sum\nolimits_c \frac{\varphi_c}{N_c Q_c}\int_{f_c}^{1} ds q_c(r,s) q_c^+(r,s), \tag{7}$$

where φ_c is the volume fraction of component c in the blend. The partition function of the single chain Q_c is

$$Q_c = \frac{1}{V}\int_V dr q_c(r,1). \tag{8}$$

The above set of equations [Eqs. (1)–(8)] is solved self-consistently using the pseudo-spectral method and the code developed by Morse and co-workers.[17] The ω fields are initially guessed and expanded in a symmetry-adapted basis function based on the morphology for which the free energy is to be calculated. The equations are then solved iteratively until convergence. Finally, the free energy F is evaluated as

$$\frac{F}{\rho k T} = \sum\nolimits_c \left(\frac{\varphi_c}{N_c}\left[\ln\left(\frac{\varphi_c}{Q_c}\right) - 1\right]\right) + \frac{1}{NV}\int dr \left[\phi_A \phi_B \chi N - \sum\nolimits_{i=A,B} \omega_i \phi_i\right]. \tag{9}$$

The equations are solved in dimensionless units. Different Kuhn lengths are used for the two monomers, and the results depend on the variables χ, N_c, f_c and the blend composition (φ_c).

B. Dissipative particle dynamics

Particle-based simulations account for density and composition fluctuations in the system whose effect is neglected in SCFT. Furthermore, they readily allow the analysis of spontaneously formed network phases lacking long-range order. Dissipative particle dynamics (DPD) has been introduced[18] as a coarse-graining approach to study mesoscale phenomena

at longer time and length scales than those allowed by conventional molecular dynamics. To achieve this, the potential of interaction between particles is modified and coupled with a thermostat that consists of dissipative and random forces. It has been applied successfully[19,20] to model microphase assembly of copolymer systems. Each macromolecule is modeled as a chain of beads (particles) linked by harmonic springs with the spring force given by $\boldsymbol{F}^S{}_{ij} = -k^S \boldsymbol{r}_{ij}$, where bead i is connected to bead j and spring constant $k^S = 4$ in our calculations. The interparticle interaction force between beads is given by

$$F_{ij}^C = \begin{cases} a_{ij}(1 - |r_{ij}|)\hat{r}_{ij}, & if, |r_{ij}| < 1 \\ 0, & if, |r_{ij}| \geq 1 \end{cases}, \tag{10}$$

whose range also defines the effective "bead diameter" and the unit length used to reduce all lengths reported hereafter. It should be noted that we did not incorporate bead size asymmetry in this model, and the mass, length and time scales are all set to unity. To model the differing chemical interactions between monomers of different types, the coefficient a_{ij} is defined as

$$a_{ij} = \begin{cases} 25, & i = j \\ 25 + 3.27\chi, & i \neq j \end{cases}, \tag{11}$$

where χ is the Flory-Huggins parameter. The equations of motion are integrated using a modified velocity Verlet scheme.[21] The Lowe-Andersen's thermostat[22] is used to maintain the reduced temperature fixed at unity. It acts on the relative velocity along the particles' center of masses and is designed to conserve their momentum. The overall density of the beads in the simulation box is exactly $\rho = 3$ and all simulations are carried out in the canonical (constant density, composition, and temperature) ensemble.

For each blend composition, simulations were carried out in cubic boxes for two million iterations with time step $\delta t = 0.05$; i.e., a duration of 10^5 units in dimensionless time. We only explored cubic boxes because our key interest was in identifying bicontinuous or cocontinuous phases with cubic symmetry. The range of box sizes studied was chosen taking into account that the shorter chains act as a cosurfactant and thus lower the thickness of the minority block domain resulting in smaller unit cells than those used for the pure DBC with the longer chains. Accordingly, our simulation box sizes "L_{box}" ranged from $L_{box} = 10$–25. The box size is critical because it artificially imposes a periodic length scale to the system. Cubic bicontinuous and cocontinuous phases are most affected since, e.g., for the gyroid morphology, we have to accommodate an integral number of unit cells (typically just one) in the box. This effect is milder for other phases but even for hexagonal cylinders, the tubes tend to align along the [111] direction of the simulation box. To probe the G phase at multiple box sizes, we used the final configuration obtained from simulations where it formed spontaneously and expanded or contracted the box with appropriate chain insertions and deletions to match both the overall density of $\rho = 3$ and the volume fraction of the blend. For preparing such initial configurations, an ad-hoc Monte Carlo scheme was used wherein the pressure was either reduced (to zero) for volume expansions or increased to large values (80 here) for contractions, while chain insertions/deletions, and relaxation moves were performed concurrently.

After the compression/expansion run, the configurations are further equilibrated using DPD for 2×10^6 time steps at $\delta t = 0.05$, after which the pressure (and compressibility factor) is calculated at a finer time step of $\delta t = 0.01$. Five configurations from this run are used as starting points for separate MC-EXE runs as described below.

C. Calculation of free energies

Due to the multitude of box sizes studied using DPD and the morphologies obtained at each blend composition, a reliable estimate of the free energy is crucial to determine the stable phase. To calculate the free energy, we resort to Monte-Carlo simulations in an expanded ensemble[23] (MC-EXE). The potential model used for this system is the same one used for the DPD simulations.

To calculate the chemical potential, chains are gradually added/removed, in λ_m stages, i.e., one bead at a time in this work. The transitions between these stages ($\Delta = +1$ for insertion and $\Delta = -1$ for deletion) are accepted according to the Metropolis criterion

$$P_{acc} = \min\{1, \exp(\nu + \psi_{m+\Delta} - \psi_m)\}, \tag{12}$$

where $\nu = -\Delta \ln W$, with W the Rosenbluth weight.[24] ψ_m are the biasing weights that are iteratively adjusted to attain a uniform sampling of all intermediate λ_m stages (i.e., a "flat histogram" approach). From the simulation, the free energy difference between successive stages is calculated using Bennett's acceptance ratio method[25]

$$\beta \Delta A_{m,m+1} = C - \ln \frac{l_{m+1,m}}{l_{m,m+1}}, \tag{13}$$

where $l_{m,m+1}$ is the number of transitions from λ_m to λ_{m+1} and C is calculated from

$$\sum_m \frac{1}{1 + \exp(\nu_{m \to m+1} - C)} = \sum_{m+1} \frac{1}{1 + \exp(\nu_{m+1 \to m} - C)}. \tag{14}$$

The excess chemical potential for the whole chain (each species) is simply the cumulative free energy change over these stages, i.e., $\mu^{ex} = \sum_{m=0}^{N-1} \Delta A_{m,m+1}$. Finally, the excess free energy of the system is calculated by

$$\begin{aligned} \beta a^{ex} &= \beta \sum\nolimits_c y_c \mu_c^{ex} - (Z - 1) \\ &= \beta \sum\nolimits_c \left(y_c \sum\nolimits_{m=0}^{N_c - 1} \Delta A_{m,m+1} \right) - (Z - 1), \end{aligned} \tag{15}$$

where y_c is mole fraction of component c, $Z = \beta P V/(\Sigma_c M_c)$ is the compressibility factor, M_c is the number of chains of component c, and $\beta = 1/kT$ (with k = Boltzmann's constant). Error bars in the free energy estimates (for each set of blend compositions and system sizes) were obtained as the standard

deviation of the values obtained from 5 independent simulations.

The free energies from this MC-EXE method [Eq. (15)] are expected to be suitable for the purpose of discerning the stability of different morphologies obtained at the same thermodynamic conditions. It should be pointed out, however, that for morphologies with three dimensional symmetry, like the bicontinuous phases, Eq. (15) ignores a correction needed to account for the fact that our simulations do not allow fluctuations in the number of unit cells (of the given morphology) in the system.[26,27] Such a correction is especially important to identify the optimal system size at which a phase attains its minimum free energy. In such cases, an alternative "thermodynamic integration" method "TI" is preferable to simulate free energies. With TI, we can estimate the free energy difference (of a given phase) between the desired χN and the disordered phase at $\chi N = 0$ by constructing a 3-step reversible path from the initial and final states[28] consisting of: (i) applying an ordering field of the desired morphology at $\chi N = 0$ to drive self-assembly, (ii) increasing the value of χN to the final state, and (iii) switching off the ordering field at the final value of χN. A detailed account of how this TI method is implemented (e.g., to create the ordering field) and its application to different systems is the subject of a forthcoming publication. In this paper, we will just use it for a representative case to validate the conclusions drawn from the MC-EXE results.

III. RESULTS

A. SCFT

We used SCFT in a canonical ensemble to predict the phase behavior of three binary blends in the composition range $0 \le \varphi_s \le 1$, for varying lengths of the symmetric chains. Here, φ_s is the volume fraction of the symmetric diblock copolymer chains in the mixture. It is related to the overall volume fraction of the minority block or monomer type A (φ_A) by the relation $\varphi_A = f_{as}(1 - \varphi_s) + f_s\varphi_s$. Asymmetric Kuhn lengths were used, namely, b_A:b_B = 1:1.11, to mimic PS-*b*-PI. Three lengths of the shorter diblock were studied, which are denoted in order of decreasing size as *s*1, *s*2, and *s*3. Note that since SCFT describes the behavior of chains in the infinitely long chain length limit, only relative chain length values are meaningful and we choose as reference $N_{s1} = 1$. Details of the system are found in Table I and the results are summarized in Fig. 1. The phase diagram was constructed for χN_{s1} ranging from 11 to 25 in steps of unity. This enables us to study the blends in the same temperature range, with the *as*-*s*1 blend entirely above the ODT ($\chi N_{s1} = \chi > \chi N_{\mathrm{ODT}}$). As φ_A is increased, a progression of phases from C to G to L was observed for each of the blends. At low values of χN_{s1}, the blends of *s*2 and *s*3 with large amounts of the symmetric component were in the disordered state as is expected due to the proximity of the ODT for the pure symmetric DBC. Other candidate phases included in the study were the double diamond and body-centered-cubic micellar phases, but these were found to be always unstable.

TABLE I. Chain lengths used in the SCFT study. N is the "relative" degree of polymerization and f is the fraction of monomer A in each component.

Component	N	f
as	2.866	0.185
*s*1	1	0.485
*s*2	0.79	0.455
*s*3	0.652	0.490

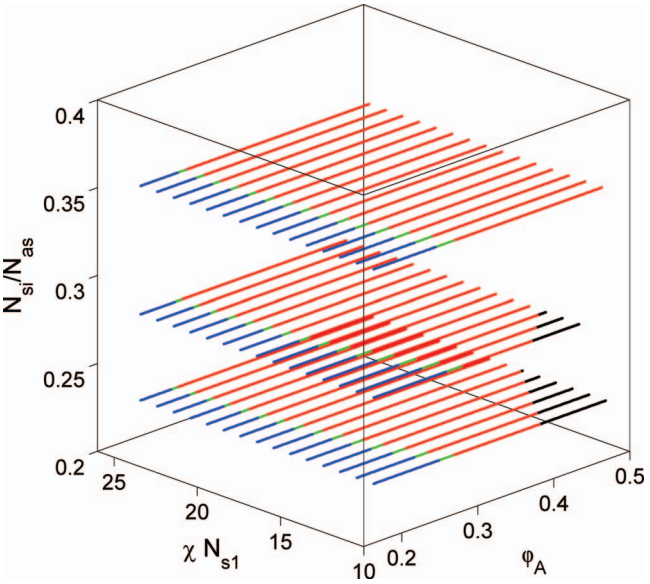

FIG. 1. Phase diagram from SCFT for blends *s*1 (top), *s*2 (middle), and *s*3 (bottom) as described in Table I. Blue = cylinders, green = gyroid, red = lamellar, black = disordered.

The predicted sequence of stable phases on increasing φ_A; i.e., C → Bicontinuous → L and the L → Disorder (for small N_{si}/N_{as}) is consistent with the experimental observations of Hashimoto and co-workers.[13] Note also that in their experiments no macrophase separation was observed for any of the blends under study. Figure 2 compares all three mixtures at the same value of χ, and the experimental data

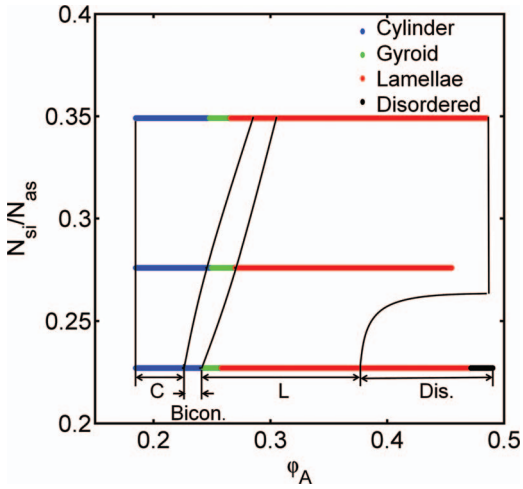

FIG. 2. Phase diagram at constant temperature ($\chi N_{s1} = 15$). The solid black lines mark the phase boundaries obtained by Court and Hashimoto.[13]

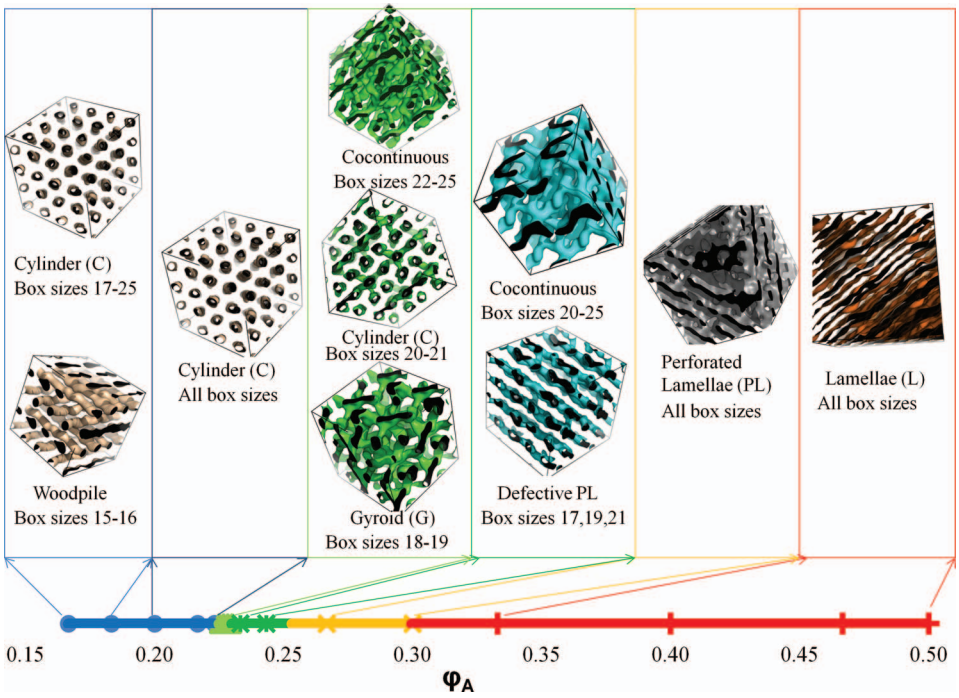

FIG. 3. Morphologies obtained $\chi N = 35$ for various blend compositions φ_A and at various box lengths. For clarity, only the interfaces between block domains are shown.

by Court and Hashimoto at room temperature. The unidentified bicontinuous (Bicon.) phase in the experiments occurs around regions in the theoretical phase space where the gyroid is stable. In the experiments, the pure asymmetric polymer yielded a BCC sphere microstructure, which we did not observe in our SCFT calculations, although the free energy of the spheres was only marginally higher than that of hexagonal cylinders. For both theory and experiment, the *as*-*s*2 blend has the widest range of stability of gyroid which may be attributed to the highest degree of asymmetry ($f = 0.455$) in the short chain. However, there is disagreement between the theory and experiments in the location of the φ_A window where the bicontinuous phase is stable. In experiment, there is a significant shift towards higher volume fractions whereas in the theory there is hardly any shift at all (for all the values of χ explored). The reason for such qualitative difference is unclear, although it may be partially attributed to differences between the gyroid morphology of SCFT and the unresolved experimental bicontinuous morphologies.

B. DPD

We performed DPD simulations for only one of the systems studied with SCFT, the one with the longest symmetric diblocks, *s*1. This choice was set by the requirement of a moderate chain length for the long asymmetric DBC to keep the system size computationally tractable; accordingly, a too-short symmetric DBC would have entailed the use of unrealistically few beads in that chain. For the asymmetric chain, the number of beads per chain is $N_{as} = 18$ and the fraction of beads of type A is $f_{as} = 1/6$. For the symmetric chain, the chain length is $N_s = 6$ and the fraction of A-type monomers is $f_s = 0.5$. This results in both types of chains having the same number of A-type beads (=3). The systems were simulated at a value of $\chi N_s = 35$, hereafter simply denoted as χN, and for different values of blend composition φ_s, which is the volume fraction of the short, symmetric chains in the blend. φ_s is varied from 0 to 1, so that the overall volume fraction of A, $\varphi_A = 1/6 + \varphi_s/3$ varies from $f_{as} = 1/6$ to $f_s = 1/2$.

The double gyroid (G) and cylinder (C) phases were formed spontaneously at relatively low values of φ_s. Other spontaneous phases that were observed during the course of these simulations were the simple cubic woodpile (W) phase,[29] perforated lamellar (PL) phase, lamellar phase (L), and various cocontinuous networks whose symmetry could not be ascertained. Snapshots of spontaneously appearing microphases are shown in Fig. 3.

At $\varphi_A = 0.167$ ($\varphi_s = 0$), we observe hexagonally arranged cylinders (C) for moderate values of box size ($17 \leq L_{box} \leq 25$). For small box sizes ($15 \leq L_{box} \leq 16$), we observe a 2-layer woodpile phase (W). To our knowledge, this phase has never been reported in simulations (a four-layer woodpile structure was recently reported in experiments[29]). In this phase, cylinders of alternating layers point in perpendicular directions with the two layers repeating periodically.

Figure 4 shows the calculated free energies for the woodpile and C phases for a blend composition of $\varphi_A = 0.1833$. Although the stable phase could not be resolved from this plot given the proximity of free energy minima and the size of the error bars, finite size effects are likely more significant for the woodpile phase which only occurs for small boxes. For $L_{box} = 15$ at which the woodpile phase has the lowest free energy, it remains stable for over 10 million steps. Once formed, there are likely both a considerable kinetic barrier and a stabilizing finite size effect (from the tubes connecting through the box periodic boundaries) to allow the reorientation of tubes into a

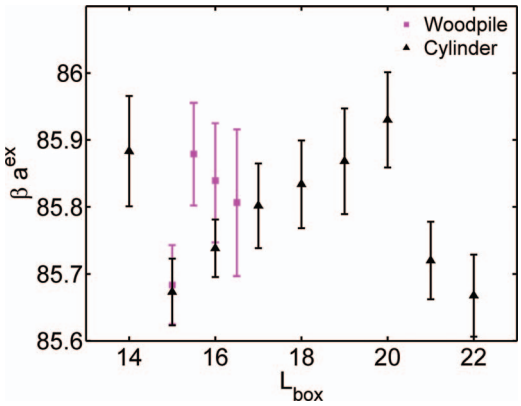

FIG. 4. Variation of free energies of the woodpile and cylinder phases with box size at blend composition $\varphi_A = 0.1833$. The error bars give the standard deviation of the data.

hexagonally arranged C structure. On doubling the box size, the woodpile phase undergoes a transition to the C phase in fewer than one million steps, further supporting the idea that the woodpile phase is metastable with respect to the cylinder phase.

The woodpile phase continued to appear at smaller box sizes for values of φ_A up to 0.2167 ($\varphi_s = 0.15$). For the rest of the box sizes only cylindrical morphologies formed, albeit with the appearance of more defects as φ_A increased. These defects included necking of cylinder tubes and the formation of loops, branched nodes, and in some cases, undulating tubes.

For $\varphi_A = 0.2267$ ($\varphi_s = 0.18$), we first observed a G morphology that emerged spontaneously for $L_{box} = 19$. In this vicinity, we ran simulations at finer intervals in φ_A. The G phase appeared spontaneously for $\varphi_A = 0.2250$, 0.2267, 0.2283, and 0.2300 in competition with both the C phase and cocontinuous network structures. A discussion of the free energy results and stability of these phases is described in detail in Sec. III C.

Between $\varphi_A = 0.2333$ ($\varphi_s = 0.20$) and $\varphi_A = 0.2433$ ($\varphi_s = 0.23$) no clear symmetry of the morphologies could be identified for any box size. A dominating feature of these morphologies was the prevalence of single networked structures, instead of the two interweaving networks characteristic of bicontinuous phases. Since both the majority and minority phases were continuous, these network phases were termed cocontinuous. Upon increasing φ_A to 0.2667 ($\varphi_s = 0.3$), we observed perforated lamellar structures (PL) for most of the box sizes investigated. It should be noted that these perforations were not always hexagonally arranged but were more of a random nature. At $\varphi_A = 0.3$ ($\varphi_s = 0.4$), the PL phase was observed for most box sizes, with the L phase appearing for smaller box sizes. Up to $\varphi_A = 0.4$ ($\varphi_s = 0.7$), the L phase competed with the PL phase. However, for $\varphi_A = 0.4$, the perforations were tiny and dynamic, appearing and disappearing throughout the lamellae. We therefore concluded that the phase observed is indeed the L phase and the perforations are just a transient feature of the morphology. Upon increasing φ_A, the perforations disappeared entirely and we get a perfect L phase.

To map out in more detail the conditions at which the G phase emerges, further simulations were run by varying χN in steps of 5 in the vicinity of 35. A summary of our findings is presented in Table II. For $\chi N = 30$ only the PL and C phases appear spontaneously. For $\chi N = 40$, we again observe the G phase, but in a narrower window than for $\chi N = 35$, and for larger values of χN values, the G phase altogether disappears.

It should be noted that for the model adopted in the DPD simulations, the order-disorder transition (ODT) occurs at $\chi N_{\mathrm{ODT}} \sim 28$ and hence our choice of χN would put the *as-s*2 blend near the vicinity of the ODT and the *as-s*3 blend below the ODT, which is qualitatively similar to the experimental conditions. At $\chi N = 35$, $(\chi N - \chi N_{\mathrm{ODT}})/\chi N_{\mathrm{ODT}} = 0.25$, which would correspond to a χN of 13.125 for SCFT (a value included in the results of Fig. 1). Note that differences between the simulated and theoretical phase diagrams are caused not only by the difficulties in exactly mapping model parameters but more importantly by the effect of local fluctuations and finite chain length which are not accounted for in the theory.

C. Stability of the G phase

The G phase appeared spontaneously for certain box lengths at compositions between $\varphi_A = 0.225$ and $\varphi_A = 0.230$. At the same volume fractions, we also found the C phase at slightly larger box sizes, and cocontinuous morphologies at even larger box sizes. The cylinder morphologies were not all defect-free, with some necking between some cylinders. For some box sizes, the defects occurred throughout the tubes and led to a cocontinuous network. To classify the observed morphologies, the structure factor was calculated from[30]

$$S(q) = \frac{\left(\sum_j \cos q \cdot r_j\right)^2 + \left(\sum_j \sin q \cdot r_j\right)^2}{M}, \qquad (16)$$

where $\boldsymbol{r}_j$ is the position vector for beads of the minority block and M is the total number of all beads in the system. For the morphologies labeled as the G phase, the peaks in $S(\boldsymbol{q})$ occurred at positions consistent with the ratios $\sqrt{6}$:$\sqrt{8}$:$\sqrt{14}$:

TABLE II. Morphologies obtained using DPD by varying χN for blend compositions $0.2233 \leq \varphi_A \leq 0.2300$. "Def" refers to morphologies with defects, C = cylinders, G = gyroid, PL = perforated lamella, and Cocon. = concontinuous phase.

χN	$\varphi_A = 0.2233$	$\varphi_A = 0.2250$	$\varphi_A = 0.2267$	$\varphi_A = 0.2283$	$\varphi_A = 0.2300$
30	Def C	Def C/def PL	Def C/def PL	Def C/def PL	Def C
35	C	G, C, cocon.	G, C, cocon.	G, C, cocon.	G, C, cocon.
40	PL, C	G, C, cocon.	G, C, cocon.	PL, C, cocon.	PL, C, cocon.
45	C	Cocon.	PL, C	...	Def PL

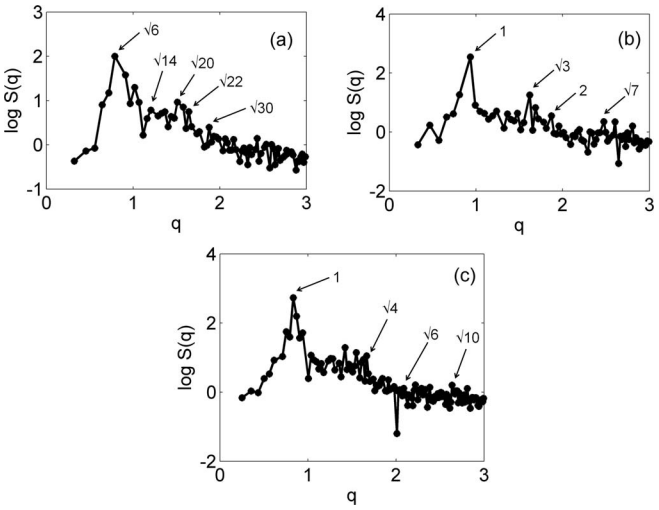

FIG. 5. Structure factor of each of the (a) gyroid for $L_{box} = 19.5$, $\varphi_A = 0.2250$, (b) cylinders for $L_{box} = 19$, $\varphi_A = 0.2250$, and (c) cocontinuous phase for $L_{box} = 25$, $\varphi_A = 0.2267$.

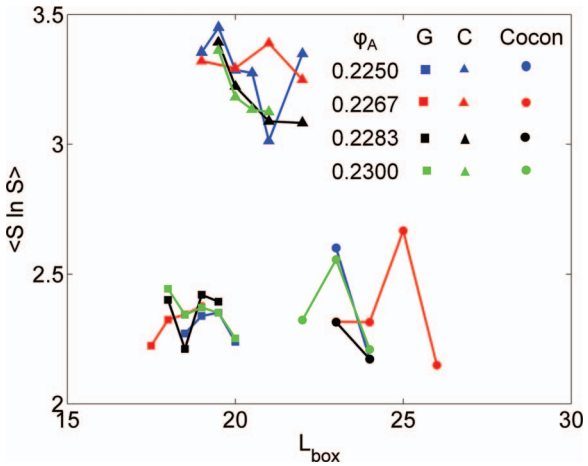

FIG. 6. Order parameter Q as a function of box size for the gyroid, cylinders and cocontinuous morphologies for blend compositions $0.2250 \leq \varphi_A \leq 0.2300$; $\chi N = 35$.

$\sqrt{16}$:$\sqrt{20}$:$\sqrt{22}$:$\sqrt{24}$:$\sqrt{26}$:$\sqrt{30}$:$\sqrt{32}$:$\sqrt{38}$:$\sqrt{42}$,[31] although not all of them were always present prominently. An example is plotted in Fig. 5(a) for a snapshot taken at $\varphi_A = 0.2250$. For the C phase, we get peaks consistent with the ratios $\sqrt{1}$:$\sqrt{3}$:$\sqrt{4}$:$\sqrt{7}$, indicating a hexagonal ordering (Fig. 5(b)). Figure 5(c) shows peaks of a cocontinuous phase in the ratios $\sqrt{1}$:$\sqrt{4}$:$\sqrt{6}$:$\sqrt{10}$, which are inconsistent with any known cubic bicontinuous phase; these phases are termed as disordered cocontinuous because often the square of the peak wavelengths is not in integral ratios.

Visual inspection of snapshots and structure factors proved inadequate to characterize a particular type of order in cocontinuous phases; e.g., to determine whether it is a highly defective C phase or not. To try to characterize the order in these cocontinuous phases, we used the order parameter given by $Q = \int dq\, S(q) \ln S(q)$, which measures the amount of order in the system[13](here $S(q)$ is the structure factor for the type A monomers in the system). This order parameter is therefore akin to the negative of an "entropy" in the structure factor. In general, it is expected to be highest for the lamellar phases, somewhat lower for hexagonal cylinders and perforated lamellae, even lower for bicontinuous and cocontinuous phases (as the number of peaks contributing to the structure increases), and is zero for the disordered phase. The results are plotted in Fig. 6 for $\chi N = 35$. It is seen that the G phases have much lower values than the C phases, whereas some of the cocontinuous morphologies are more network-like while others have some cylinder-like character. This order parameter was used to distinguish perforated lamellae from cocontinuous phases for blend compositions in the $0.2333 \leq \varphi_A \leq 0.2433$ range.

For the blend composition $\varphi_A = 0.230$, the simulated free energy via MC-EXE is plotted against simulation box size in Figure 7(a). Changes in free energy with box size are most pronounced in the G phase (observed in other blend compositions as well). In contrast, the average free energies of the cocontinuous phases seem the least sensitive to box size. Figure 7(b) shows the free energy relative to $\chi N = 0$ for the gyroid and cylinder phases using the TI method. Note that the TI results exhibit error bars (O(0.01)) that are much smaller than those for the MC-EXE method (O(0.1)), and that (at least in this case) the MC-EXE and TI results are consistent in that: (i) the free energies of the cylinder and gyroid phase are within error bars of each other and (ii) the free energy minimum for a given phase occurs at the same box size (L_{box}). In view of this and that the TI method would be difficult to apply to get free energies for the disordered cocontinuous phases,

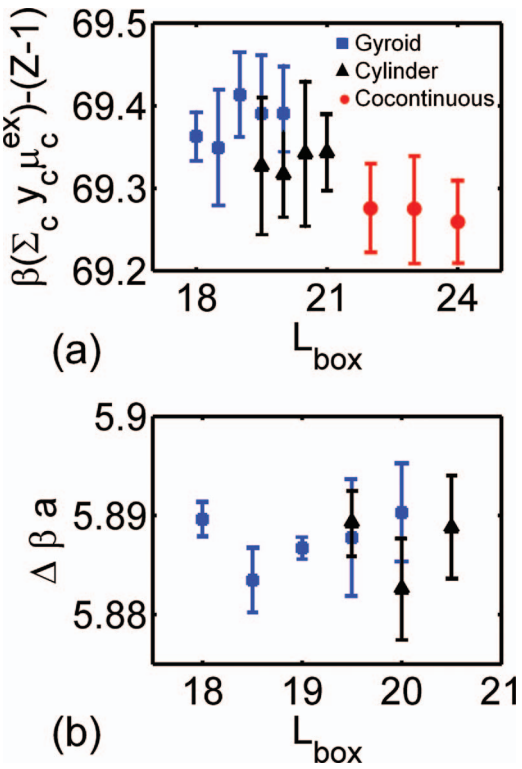

FIG. 7. Variation of free energy with box size for different morphologies for blend composition $\varphi_A = 0.230$ and $\chi N = 35$: (a) from MC-EXE method and (b) from TI method (showing free-energy difference relative to the $\chi N = 0$ system).

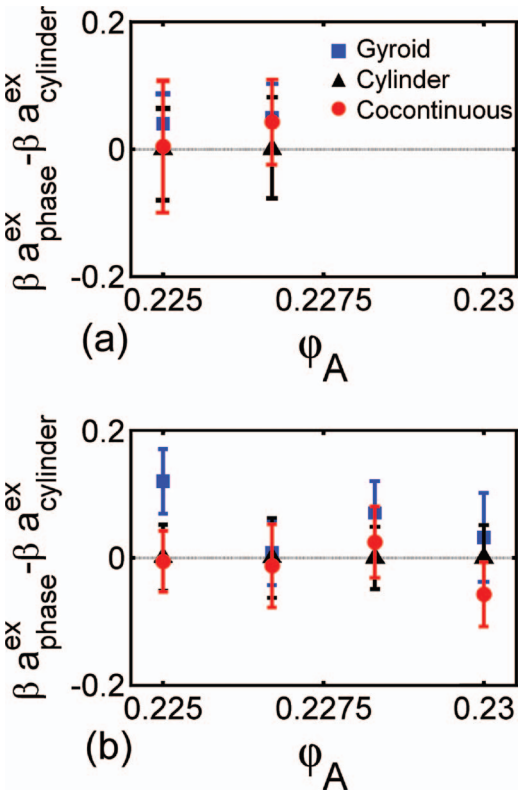

FIG. 8. Free energies of the gyroid and cocontinuous phases relative to that of the cylinder phase for various blends at (a) $\chi N = 40$, (b) $\chi N = 35$.

we will henceforth only discuss results obtained via the MC-EXE method.

For a given set of conditions (χN and blend composition), the stable phase is the one which has the lowest free energy among all box sizes. Figure 8 gives the lowest free energy of each phase relative to that of the cylinder phase for the range of φ_A studied. One can see that the free energies for the three competing phases are within error bars of each other for all blend compositions, and variations in simulation initial conditions might lead to the appearance of one phase or another (even if only as a long-lived metastable state). Furthermore, with free energies so close together, multi-phase coexistence is a possibility (a scenario that could not be directly explored due to the small box sizes used for computational expediency). It is conjectured that similar metastability issues and partial phase transformations may have contributed to the difficulty in identifying the "bicontinuous" structure observed in the experiments of Court and Hashimoto.[13]

We also examined the effect of box size on the contributors to the free energy [as per Eq. (15)]. The compressibility factor (Z) and therefore the pressure tend to decrease slightly upon increasing box size, suggesting that larger box sizes may help relieving some mechanical stress associated with the orientation or compatibility of the morphological patterns in the simulation box. In contrast, the chemical potential for each component does not follow any particular trend among all blend compositions studied (results not shown), thus indicating a non-trivial dependence of the free energy of such contributors. We also calculated the end-to-end distances for both the asymmetric and symmetric chains in all

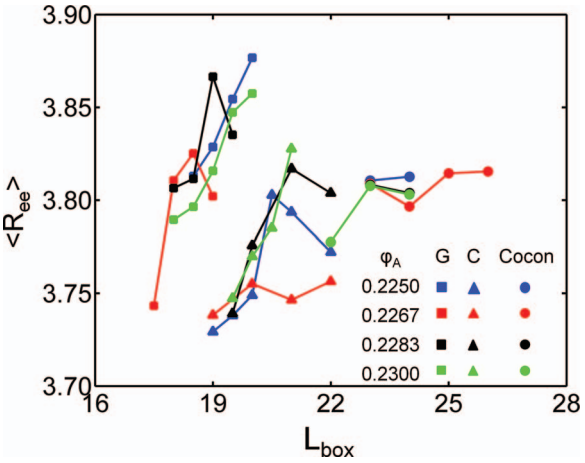

FIG. 9. End-to-end distances for B block of asymmetric chains *as*.

morphologies. For the G phase, as box size increases, the end-to-end distance of the asymmetric chains *as* increases; this is true for the overall chain and for the individual A and B blocks within *as*. These data are shown in Fig. 9 for $\varphi_A = 0.230$. On the other hand, the end-to-end distances of the symmetric chains *s*1 of all morphologies lie within the same range of values (~1.295–1.315 data not shown). This is expected, as shorter chains are known to act as "stiffer" entropic springs. It is then the extension of the longer (15-bead) B blocks in the *as* component that is expected to have a larger contribution to conformational entropy in the system and serve as a probe of the degree of confinement in the B-rich domain. The fact that for all morphologies the *as*-B block end-to-end distance tends to decrease upon reducing the box size reflects a concomitant decrease in the B-domain "thickness" that accentuates the confinement of the enclosed chains. However, this trend need not be monotonous (e.g., if the domain geometry does not scale affinely with L_{box}) and is strongly dependent on morphology (e.g., chain extension in the disordered cocontinuous phases seems the least sensitive to box size).

Figure 9 also shows that the C phase is the one that achieves the lowest level of chain stretching (for a suitable choice of box size). Because chain stretching is a hallmark of packing frustration, these observations suggest that one should also observe regions of lower density in the centers of the B (*majority*) block domains which the *as*-B block chains are trying to fill (driving their over extension). This expectation is verified in Fig. 10 which shows the spatial variation of the B-block density and where one can see lower density regions (green) in the center of the B-domain. Indeed, one also sees that the low B-density pockets increase going from the C, to the G and to the cocontinuous phases, in correspondence to their average *as*-chain end-to-end distances under those conditions. While packing frustration is the result of morphology-specific competition of enthalpic interactions (trying to minimize the interfacial surface area) and entropic interactions that favor uniform mixing and density, it is likely that the disparity in the B-block lengths enhances packing frustration in the B domain. Note that since the SCFT we used before (in Sec. III A) assumes uniform domain densities and Gaussian

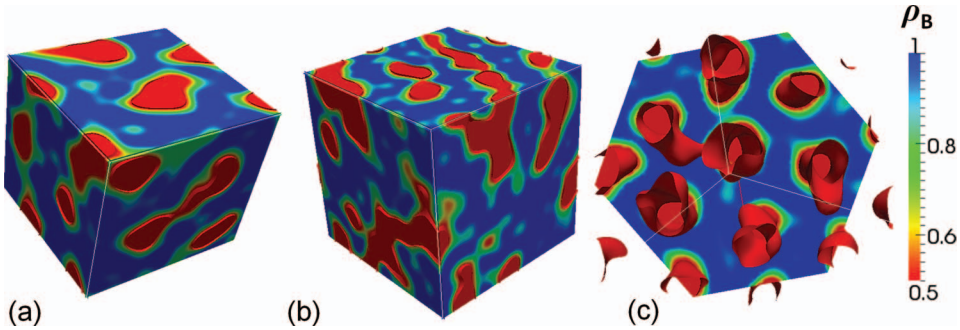

FIG. 10. Local density of the majority domain. Red portions indicate regions of the minority domain. Green (low density) pockets in the "bulk" of the blue domain evidence packing frustration. (a) Gyroid phase for $L_{box} = 19.5$, $\varphi_A = 0.2250$, (b) cocontinuous phase for $L_{box} = 25$, $\varphi_A = 0.2267$, and (c) cylinder phase for $L_{box} = 19$, $\varphi_A = 0.2250$.

chain behavior, it is not suitable to capture the chain stretching behavior and the local lower density regions as described in Figs. 9 and 10.

Finally, we examined the spatial distribution of chains in the A (minority) domain and around the block interfaces to detect any signs of morphology-dependent packing frustration or local segregation. No regions of lower density are detectable in the A domains (results not shown), perhaps a consequence of the short A blocks and the thin tubes or struts involved. The structure factors of each of the components indicate that there is no preferential arrangement towards nodes or tubes for the longer chains (results not shown) and that the interface is shared evenly between the two components (see Fig. 11(a)). However, the A-B junctions of the longer, asymmetric chains are more confined within the minority domain while the A-B junction of the shorter, symmetric chains occupies the domain periphery in the G (see Fig. 11(b)), C, and cocontinuous phases. In a sense, two parallel interfaces emerge having the same morphology separated by a small distance (equal or less than one bead diameter), with the shorter chains occupying the one with the lower curvature. These results are surprising in that one may have expected the outer interface to be formed by the asymmetric chains since these are being "pulled" toward the centers of the B domains (i.e., the packing frustration of their B-blocks). We conjecture that it is the shorter symmetric chains that form the outer interface because in this way (i) they are less confined at the interface and hence lose less translational and mixing entropy and (ii) the *packing frustration in the narrow A domains* is alleviated. Interface "shifting" could then be seen as an alternative strategy to fill the A-domain uniformly when chain stretching is too demanding and minimal (as with the short A-blocks used here). As blend composition is increased and the curvature of the A-B interface decreases, we find that these two interfaces almost coincide and for the perforated lamellae, these are essentially identical.

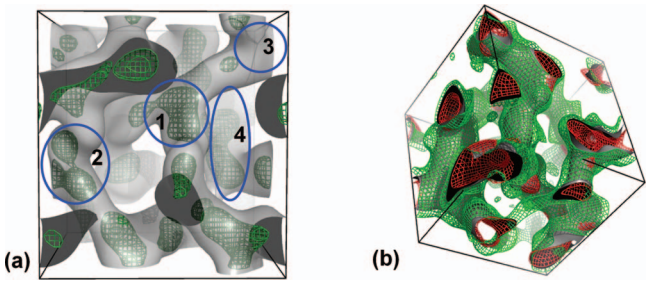

FIG. 11. Isosurfaces of A-block fraction = 0.5 for the gyroid phase with $L_{box} = 19.5$, $\varphi_A = 0.2250$: grey surface represents overall A-monomers in the blend, green mesh for symmetric chains, and red mesh for asymmetric chains. (a) Density calculated as the *number of symmetric chain A beads over total number of beads*. Points 1 and 2 show nodes that the symmetric chains occupy, 3 is a node which such chains do not occupy, and 4 refers to a tube of the that such chains occupy. (b) Density calculated as *number of A beads of all chains over total number of beads.*

IV. CONCLUSIONS

In this work, we have shown that for a binary blend of DBCs containing a longer cylinder-forming asymmetric DBC and a shorter lamellae-forming symmetric DBC, the phase diagram reveals the progression from a cylinder to a lamellar phase with an intermediate morphology. Although SCFT calculations predict that the gyroid phase is stable over a narrow composition range of the blend, particle-based simulations indicate that in such a region the free energy of the gyroid, cylinder, and disordered cocontinuous phases are within error bars of each other, even for different values of χ. Further examination of the structure factor and chain spatial distributions show that both types of DBCs occupy the interface evenly; e.g., they do not preferentially reside in the nodes or the struts of the gyroid phase. However, the shorter chains penetrate less and the longer chains penetrate more into the minority domain, creating a "double" interface that likely relieves packing frustration in the A-rich phase but contributes to packing frustration in the B-rich phase. Such chain stretching and interface shifting can be seen as mechanisms by which the system can realize a given morphology minimizing the loss in chain conformational entropy (by extending mostly the more forgiving longer chains) and in translational entropy (by reducing the confinement of the shorter chains). In the future, it will be interesting to explore the feasibility of using an asymmetric DBC additive but of a composition chosen to alleviate packing frustration in both of the domains; depending on the length and composition of such an additive, it could stabilize a gyroid phase over a broader range of conditions and at

overall A-block volume fractions that may be lower or higher than those where it is observed in pure DBCs.[32]

An intriguing finding in this work is the appearance of a metastable woodpile phase. Although its free energy was found to be within error bars of the cylindrical phase, the woodpile phase transforms to a cylinder phase when the box size is doubled in each dimension. In spite of this, the fact that the woodpile phase appears spontaneously seems to indicate that its stability could be achieved not far from the composition space explored in this work. Some of our ongoing work entails precisely exploring DBC blends and conditions where the woodpile phase becomes stable. A related but broader area of interest relates to understanding how the preparation and processing conditions (e.g., via the use of transient external forces and flows) could bias the system to be kinetically trapped in a desired metastable phase among a number of competing phases having similar free energies (e.g., to trap the woodpile phase at compositions where it competes with a stable C phase, or to form the G phase at conditions where it competes with the C and cocontinuous phases).

Finite size effects associated with small box sizes constitute one of the important shortcomings of particle-based simulations. In principle, for periodic ordered morphologies one should consider using ensembles where the number of unit cells is increased until attaining a limiting convergent behavior. Ongoing work focuses on determining the true unit cell size of the morphologies by indirect estimation of the "chemical potential" associated with number of unit cells[26] from calculations of free energy using thermodynamic integration[27] and those of chemical potentials and compressibility factors using the methods described in this paper. In the case of ordered, orthorhombic cocontinuous phases, one should consider varying not only the system size but also the asymmetry of the box sides to attain the optimal unit cell shape (which need not be the same as the theoretical one). Constant pressure simulations, as opposed to constant density simulations, could also help discriminate the most stable phase at conditions where competing phases may lead to non-negligible differences in density. Clearly, such undertakings would entail large investments of computational resources and advocate for alternative hybrid approaches, like the one adopted here, where the results and strengths of SCFT and particle-based simulations are combined to probe both large system-size behavior (via SCFT) and crucial details of the local structure of selected phases (via DPD).

ACKNOWLEDGMENTS

This work was supported by Grant CBET 0756248 from the National Science Foundation. This publication is also based on work supported in part by Award No. KUS-C1-018-02, made by King Abdullah University of Science and Technology (KAUST). F.J.M.V. was supported by the ERC (Advanced Grant Agreement No. 227758). We are thankful to Professor David Morse from University of Minnesota for the code for implementing SCFT.

[1] V. Saranathan *et al.*, Proc. Natl. Acad. Sci. U.S.A. **107**, 11676 (2010).
[2] A. S. Zalusky, R. Olayo-Valles, J. H. Wolf, and M. A. Hillmyer, J. Am. Chem. Soc. **124**, 12761 (2002).
[3] E. J. W. Crossland *et al.*, Nano Lett. **9**, 2807 (2009).
[4] M. W. Matsen and F. S. Bates, Macromolecules **29**, 7641 (1996).
[5] M. W. Matsen, J. Phys.: Condens. Matter **14**, R21 (2002).
[6] C. A. Tyler and D. C. Morse, Phys. Rev. Lett. **94**, 208302 (2005).
[7] M. I. Kim *et al.*, Macromolecules **42**, 5266 (2009).
[8] A. Shi and J. Noolandi, Macromolecules **27**, 2936 (1994).
[9] M. W. Matsen and F. S. Bates, Macromolecules **28**, 7298 (1995).
[10] M. W. Matsen, Macromolecules **36**, 9647 (2003).
[11] Z. Wu, B. Li, Q. Jin, and D. Ding, Macromolecules **44**, 1680 (2011).
[12] R. J. Spontak, Macromolecules **29**, 4494 (1996).
[13] F. Court and T. Hashimoto, Macromolecules **34**, 2536 (2001).
[14] F. Chen, Y. Kondo, and T. Hashimoto, Macromolecules **40**, 3714 (2007).
[15] P. M. Lipic, F. S. Bates, and M. W. Matsen, J. Polym. Sci., Part B: Polym. Phys. **37**, 2229 (1999).
[16] F. J. Martinez-Veracoechea and F. A. Escobedo, Macromolecules **38**, 8522 (2005).
[17] D. Morse, C. Tyler, A. Ranjan, J. Qin, and R. Thiagarajan, see http://www.cems.umn.edu/research/morse/code/pscf/home.php.
[18] J. M. V. A. Koelman and P. J. Hoogerbrugge, Europhys. Lett. **19**, 155 (1992).
[19] R. D. Groot, T. J. Madden, and D. J. Tildesley, J. Chem. Phys. **110**, 9739 (1999).
[20] F. J. Martinez-Veracoechea, and F. A. Escobedo, J. Chem. Phys. **125**, 104907 (2006).
[21] P. B. Warren and R. D. Groot, J. Chem. Phys. **107**, 4423 (1997).
[22] C. P. Lowe, Europhys. Lett. **47**, 145 (1999).
[23] F. A. Escobedo and J. J. de Pablo, J. Chem. Phys. **103**, 2703 (1995).
[24] D. Frenkel and B. Smit, *Understanding Molecular Simulation: From Algorithms to Applications*, 2nd ed. (Academic, San Diego, CA, 2002).
[25] C. H. Bennett, J. Comput. Phys. **22**, 245 (1976).
[26] W. C. Swope and H. C. Andersen, Phys. Rev. A **46**, 4539 (1992).
[27] M. Mladek, P. Charbonneau, C. N. Likos, D. Frenkel, and G. Kahl, J. Phys.: Condens. Matter **20**(49), 494245 (2008).
[28] M. Mueller and K. C. Daoulas, NIC Ser. **38**, 255 (2008).
[29] G. E. S. Toombes *et al.*, Macromolecules **41**, 852 (2008).
[30] A. J. Schultz, J. Genzer, and C. K. Hall, Macromolecules **40**, 2629 (2007).
[31] T. H. Epps III, E. W. Cochran, T. S. Bailey, R. S. Waletzko, C. M. Hardy, and F. S. Bates, Macromolecules **37**, 8325 (2004).
[32] S. Sakurai, H. Irie, H. Umeda, S. Nomura, H. H. Lee, and J. K. Kim, Macromolecules **31**, 336 (1998).